catalysts

MDPI

Article

Solvent Coordination Effect on Copper-Based Molecular Catalysts for Controlled Radical Polymerization

Stefano Racioppi [1,2], Laura Orian [1,*], Cristina Tubaro [1], Armando Gennaro [1,†] and Abdirisak Ahmed Isse [1,*]

[1] Dipartimento di Scienze Chimiche, Università Degli Studi di Padova, Via Marzolo 1, 35131 Padova, Italy
[2] Department of Chemistry, State University of New York at Buffalo, Buffalo, NY 14260-3000, USA
* Correspondence: laura.orian@unipd.it (L.O.); abdirisak.ahmedisse@unipd.it (A.A.I.)
† Deceased on 13 April 2022.

Abstract: The equilibrium of copper-catalyzed atom transfer radical polymerization was investigated in silico with the aim of finding an explanation for the experimentally observed solvent effect. Various combinations of alkyl halide initiators and copper complexes in acetonitrile (MeCN) and dimethyl sulfoxide (DMSO) were taken into consideration. A continuum model for solvation, which does not account for the explicit interactions between the solvent and metal complex, is not adequate and does not allow the reproduction of the experimental trend. However, when the solvent molecules are included in the coordination sphere of the copper(I,II) species and the continuum description of the medium is still used, a solvent dependence of process thermodynamics emerges, in fair agreement with experimental trends.

Keywords: copper complexes; nitrogen ligands; DFT calculations; solvent coordination

Citation: Racioppi, S.; Orian, L.; Tubaro, C.; Gennaro, A.; Isse, A.A. Solvent Coordination Effect on Copper-Based Molecular Catalysts for Controlled Radical Polymerization. *Catalysts* **2022**, *12*, 1656. https://doi.org/10.3390/catal12121656

Academic Editor: Aleksander Filarowski

Received: 5 November 2022
Accepted: 13 December 2022
Published: 16 December 2022

1. Introduction

Atom transfer radical polymerization (ATRP) is a controlled radical polymerization technique characterized by a unique mechanism to control the growing chains, allowing for the synthesis of polymers with narrow molecular weight distribution, well-defined composition and controlled architectures [1–3].

In Scheme 1, we present the typical mechanism of conventional ATRP. The process is based on a dynamic equilibrium between a dormant species ($P_n - X$) and a propagating polymer chain ($P_n^{\bullet}$) and is catalyzed by a transition metal complex. A large variety of metal complexes with good catalytic properties for ATRP are known. Very often, however, copper complexes with polydentate amine ligands (L) are used [4]. Polymerization is triggered by the reaction of a metal catalyst at a low oxidation state (e.g., $[Cu^{I}L]^{+}$) with an alkyl halide used as an initiator (RX). This activation step occurs via an inner-sphere electron transfer or atom transfer mechanism [5–7], yielding a propagating radical together with the metal complex at a higher oxidation state (e.g., $[XCu^{II}L]^{+}$). The radical ($P_n^{\bullet}$) is rapidly deactivated back to a dormant state ($P_n - X$) through the transfer of the halogen atom from the metal catalyst. Usually, the initiator is more active than the dormant species, so all RX molecules are converted to $P_n - X$ at the beginning of the reaction. Chains then grow at the same rate, leading to a polymer with a narrow molecular weight distribution. One of the main characteristics of ATRP is that the equilibrium constant K_{ATRP} is << 1, hence, the equilibrium is shifted towards the reactants, minimizing the rate of radical termination [8,9].

A drawback of copper-catalyzed traditional ATRP is that it requires starting with a high concentration of O_2-sensitive $[Cu^{I}L]^{+}$. Besides the necessity of using an appropriate experimental setup such as a Schlenk line to preserve $[Cu^{I}L]^{+}$ stability, the catalyst must be removed from the polymer at the end of the reaction. Several advanced ATRP techniques have been developed in the last two decades to overcome this problem [10]. They all start with O_2-stable $[Cu^{II}L]^{2+}$ or $[XCu^{II}L]^{+}$ at a very low concentration, with the

(re)generation of the $[Cu^{I}L]^{+}$ activator complex by using chemical reducing agents (ARGET ATRP) [11–13], metallic copper (SARA ATRP) [14–16], traditional radical initiators (ICAR ATRP) [17,18] or external stimuli such as photochemistry [19–21], electrochemistry [22–26] or sonochemistry [27].

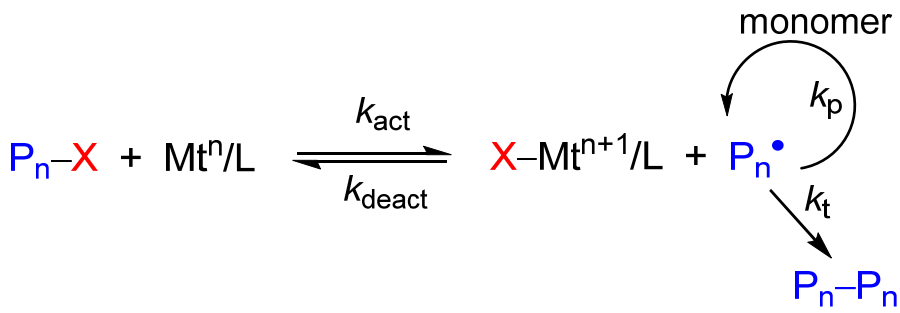

Scheme 1. General mechanism of traditional ATRP.

The equilibrium constant, K_{ATRP}, provides an excellent measurement of the activity of a given catalyst/initiator couple [9]. Several parameters influence the equilibrium constant, such as the nature of the ligand [4,8,9,28,29], the type and structure of the alkyl halide [9] and the reaction conditions (solvent, temperature and pressure) [30–34]. The solvent, in particular, appears to have greater effect on ATRP compared to other radical reactions. Indeed, the solvent affects the redox properties of copper catalysts, their structure in solution and the kinetics of activation reactions, all of which contribute to the dependence of K_{ATRP} on the reaction medium [32,35].

The thermodynamic and the kinetic aspects of ATRP have been investigated with computational methods during the past years, focusing in particular on the ligand, initiator and transition metal atom [5,36–39]. Although a lot of effort has been invested in understanding the mechanism of copper-catalyzed ATRP, some important details remain elusive [5]. Among these, the identification of the transition state is still unreached because of the variation in the multiplicity of spin that characterizes the passage from the reagents to the products and vice versa. Moreover, an exhaustive explanation of the solvent effect on K_{ATRP} is missing, even if deeply investigated experimentally [23,40]. In particular, the role of the solvent on the optimal geometry of both the activator and deactivator complexes, i.e., $[Cu^{I}L]^{+}$ and $[XCu^{II}L]^{+}$, respectively, is not clear. In order to shed some light on some of these open questions, especially the role of polar organic solvents, we present the results of a computational investigation on K_{ATRP} for some well-known copper complexes that are commonly used as catalysts in ATRP in two selected solvents, namely, acetonitrile (MeCN) and dimethyl sulfoxide (DMSO). These solvents were chosen not only because they are among the most used polar media for ATRP processes but also because experimental data on K_{ATRP} are available for them, especially in MeCN. Additionally, although both are very polar solvents, a strong difference in K_{ATRP} has been reported [30]. Therefore, they were picked as the best candidates for a computational study aiming to shed light on the role of the solvent on ATRP activation/deactivation equilibrium.

Six alkyl halides RX (R = methyl-2-propionate (MePr), ethyl α-isobutyrate ($Et^{i}Bu$) and allyl (Al); X = Cl, Br) together with three ligands, namely, tris [2-(dimethylamino)ethyl]amine (Me_6TREN), tris(2-pyridylmethyl)amine (TPMA) and *N*,*N*,*N′*,*N′′*,*N′′*-pentamethyldiethylenetriamine (PMDETA) were chosen for this study (Chart 1).

The Cu complexes are labeled as $[Cu^{n}LX_z]^{n-z}$, where n indicates the oxidation state of copper(I or II), L denotes one of the three ligands here considered, i.e., Me_6TREN, PMDETA and TPMA, and X is a halide ion, i.e., chloride or bromide. The total charge of the complex (n–z) can be +1 or +2, obtained as the difference between the copper oxidation state and the number of halide ions coordinated to the metal center.

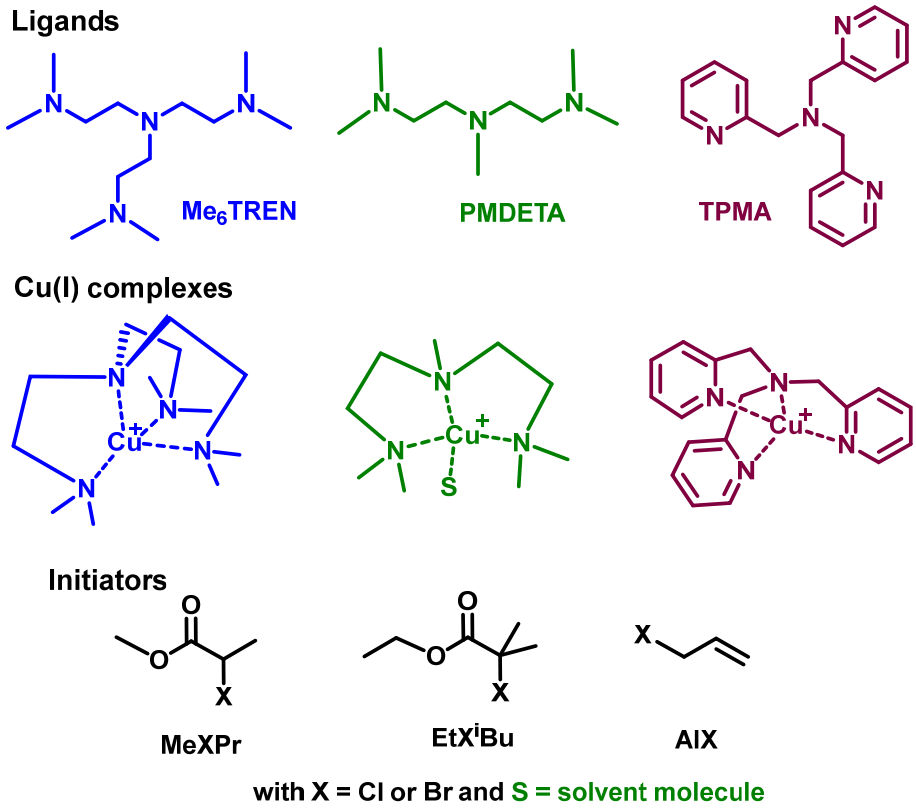

Chart 1. Chemical structures of ligands, their complexes with Cu(I) and alkyl halide initiators used in this study.

2. Results and Discussion

The overall initial ATRP process described in Scheme 1 and Equation (1), can be partitioned into two fundamental steps: (i) the homolytic RX dissociation (Equation (2)) and (ii) the oxidation of the Cu^I catalyst (Equation (3)), with each step characterized by a defined equilibrium constant (e.g., K_{ATRP} for Equation (1)) [2]. The thermodynamics associated with Equation (2) have been well described in earlier works [5], revealing a relatively small effect of the solvent. Thus, we first focus on the oxidation of the copper(I) complexes (Equation (3)).

$$RX + \left[Cu^{I}L\right]^{+} \rightleftarrows \left[Cu^{II}LX\right]^{+} + R^{\bullet} \quad (1)$$

$$RX \rightleftarrows X^{\bullet} + R^{\bullet} \quad (2)$$

$$\left[Cu^{I}L\right]^{+} + X^{\bullet} \rightleftarrows \left[Cu^{II}LX\right]^{+} \quad (3)$$

2.1. Oxidation of Cu^I Complexes by the $X^\bullet$ Radical

The oxidation of the Cu^I catalyst (Equation (3)) is an important step of the ATRP mechanism [4]. This reaction involves the interaction between the halogen p_z orbital and the HOMO of the Cu^I catalyst, with the formation of a Cu-X bond with almost equivalent metal and ligand contributions (55% and 45% $[Cu^I(Me_6TREN)]^+$, 50% and 50% $[Cu^I(PMDETA)]^+$, 54% and 46% $[Cu^I(TPMA)]^+$) (Table S1). Upon oxidation, significant structural changes occur in the copper complexes, especially in the coordination number (Tables S2–S4). The calculated ΔE_r and ΔG_r values for reaction (3) in the gas phase and implicit solvent (see Materials and Methods section) are reported in Table 1.

Table 1. ΔE_r and ΔG_r (kcal/mol) of reaction (3) calculated in gas phase and in solution; level of theory: (PCM-)M06/6-311+G(d,p).

Reaction	ΔE_r	ΔG_r		
	Gas phase	Gas phase	In MeCN [1]	In DMSO [1]
$[Cu^{I}(Me_6TREN)]^+ + Cl^\bullet \rightarrow [Cu^{II}(Me_6TREN)Cl]^+$	−62.2	−51.8	−59.2	−59.3
$[Cu^{I}(Me_6TREN)]^+ + Br^\bullet \rightarrow [Cu^{II}(Me_6TREN)Br]^+$	−47.1	−37.2	−43.8	−43.9
$[Cu^{I}(PMDETA)]^+ + Cl^\bullet \rightarrow [Cu^{II}(PMDETA)Cl]^+$	−59.8	−49.6	−58.5	−58.6
$[Cu^{I}(PMDETA)]^+ + Br^\bullet \rightarrow [Cu^{II}(PMDETA)Br]^+$	−44.9	−35.5	−43.3	−43.4
$[Cu^{I}(TPMA)]^+ + Cl^\bullet \rightarrow [Cu^{II}(TPMA)Cl]^+$	−59.1	−48.9	−57.1	−57.1
$[Cu^{I}(TPMA)]^+ + Br^\bullet \rightarrow [Cu^{II}(TPMA)Br]^+$	−44.5	−34.6	−42.0	−42.0

[1] The $\Delta m RT \ln(M/0.0409)$ correction with $\Delta m = -1$, already included in the reported results, is: −3.64 kcal/mol for MeCN (19 M) and −3.46 kcal/mol for DMSO (14 M).

When $Cl^\bullet$ rather than $Br^\bullet$ is involved, the process is thermodynamically favored, in agreement with the experimental evidence [41,42]. In solution, ΔG_r values become more negative. It is to be noted that there is no appreciable difference between the reaction Gibbs free energy values computed in MeCN and DMSO. In fact, the dielectric constants of these two solvents are very similar.

To complete the whole ATRP process described in Equation (1), one must include in the oxidation process the homolytic dissociation of the carbon–halogen bond in RX (see Table 2). The reaction occurs through an atom transfer mechanism in which the carbon–halogen bond is homolytically broken while a new halogen–copper bond is formed (Scheme 2). The reaction also involves the oxidation of Cu(I) to Cu(II). As expected, both ΔE_r and ΔG_r of reaction (1), either in the gas phase or in the implicit solvent, have positive values due to the large amount of energy required for the homolytic dissociation of the initiator [9,43]. Still, no significant difference in the energetics is found between the two solvents, indicating that a continuum model for solvation is not adequate to describe the interactions between the solvent and metal complex. Hence, solvent molecules should be included explicitly

Table 2. ΔE_r and ΔG_r (kcal/mol) of reaction (1) calculated in gas phase and in solution; level of theory: (PCM-)M06/6-311+G(d,p).

Reaction	ΔE_r	ΔG_r		
	Gas Phase	Gas Phase	In MeCN	In DMSO
$[Cu^{I}(Me_6TREN)]^+ + AlCl \rightleftarrows [Cu^{II}(Me_6TREN)Cl]^+ + Al^\bullet$	7.3	6.1	1.0	0.9
$[Cu^{I}(Me_6TREN)]^+ + AlBr \rightleftarrows [Cu^{II}(Me_6TREN)Br]^+ + Al^\bullet$	8.2	7.0	2.5	2.4
$[Cu^{I}(Me_6TREN)]^+ + EtCl^{i}Bu \rightleftarrows [Cu^{II}(Me_6TREN)Cl]^+ + Et^{i}Bu^\bullet$	10.7	7.4	1.4	1.3
$[Cu^{I}(Me_6TREN)]^+ + EtBr^{i}Bu \rightleftarrows [Cu^{II}(Me_6TREN)Br]^+ + Et^{i}Bu^\bullet$	11.1	7.5	2.0	2.0
$[Cu^{I}(Me_6TREN)]^+ + MeClPr \rightleftarrows [Cu^{II}(Me_6TREN)Cl]^+ + MePr^\bullet$	12.1	10.3	4.4	4.3
$[Cu^{I}(Me_6TREN)]^+ + MeBrPr \rightleftarrows [Cu^{II}(Me_6TREN)Br]^+ + MePr^\bullet$	13.3	11.4	6.1	6.0
$[Cu^{I}(PMDETA)]^+ + AlCl \rightleftarrows [Cu^{II}(PMDETA)Cl]^+ + Al^\bullet$	9.7	8.3	1.8	1.7
$[Cu^{I}(PMDETA)]^+ + AlBr \rightleftarrows [Cu^{II}(PMDETA)Br]^+ + Al^\bullet$	10.4	8.7	3.0	2.9
$[Cu^{I}(PMDETA)]^+ + EtCl^{i}Bu \rightleftarrows [Cu^{II}(PMDETA)Cl]^+ + Et^{i}Bu^\bullet$	13.2	9.5	2.1	2.0
$[Cu^{I}(PMDETA)]^+ + EtBr^{i}Bu \rightleftarrows [Cu^{II}(PMDETA)Br]^+ + Et^{i}Bu^\bullet$	13.3	9.2	2.6	2.5
$[Cu^{I}(PMDETA)]^+ + MeClPr \rightleftarrows [Cu^{II}(PMDETA)Cl]^+ + MePr^\bullet$	14.5	12.5	5.2	5.1
$[Cu^{I}(PMDETA)]^+ + MeBrPr \rightleftarrows [Cu^{II}(PMDETA)Br]^+ + MePr^\bullet$	15.5	13.0	6.6	6.5
$[Cu^{I}(TPMA)]^+ + AlCl \rightleftarrows [Cu^{II}(TPMA)Cl]^+ + Al^\bullet$	10.3	9.0	3.2	3.1
$[Cu^{I}(TPMA)]^+ + AlBr \rightleftarrows [Cu^{II}(TPMA)Br]^+ + Al^\bullet$	10.8	9.6	4.4	4.3
$[Cu^{I}(TPMA)]^+ + EtCl^{i}Bu \rightleftarrows [Cu^{II}(TPMA)Cl]^+ + Et^{i}Bu^\bullet$	13.8	10.3	3.5	3.4
$[Cu^{I}(TPMA)]^+ + EtBr^{i}Bu \rightleftarrows [Cu^{II}(TPMA)Br]^+ + Et^{i}Bu^\bullet$	13.7	10.0	4.0	3.9
$[Cu^{I}(TPMA)]^+ + MeClPr \rightleftarrows [Cu^{II}(TPMA)Cl]^+ + MePr^\bullet$	15.1	13.2	6.6	6.5
$[Cu^{I}(TPMA)]^+ + MeBrPr \rightleftarrows [Cu^{II}(TPMA)Br]^+ + MePr^\bullet$	15.9	13.9	8.0	7.9

Scheme 2. Copper-mediated activation/deactivation mechanism in ATRP.

Nevertheless, few comments on the trends can be made in comparison with some experimental observations [9]. In terms of reaction Gibbs free energy, the reactivity of the copper(I) complexes having different ligands with the same initiator follows the order Me_6TREN > PMDETA > TPMA, whereas the experimental trend found in MeCN is Me_6TREN > TPMA > PMDETA. When considering the same ligand and the same halogen atom, the activity of the initiator changes in the order Al > Et^{i}Bu > MePr in the chloride series, and Et^{i}Bu > Al > MePr in the bromide series. The experimental findings common to RCl and RBr show the following reactivity trend: Al > Et^{i}Bu > MePr.

As regards the role of halogen atoms in the initiators, the chloro-derivatives are found to be more active than the corresponding bromo ones (Table 2), while, experimentally, it is observed that bromo-based initiators have higher K_{ATRP}, i.e., less positive ΔG_r. However, this disagreement is not due to the energy required to accomplish the sole homolytic cleavage reported in Equation (2) (see Table S5), which is in agreement with previously calculated and measured values [38,43]. The nature of the inverted trend resides in the stabilization given by the Cu–X bond formation (see Table 1), which is more favored for X = Cl than Br [41,42].

2.2. Solvent Coordination to Copper Complexes

2.2.1. Analysis of Solvent Coordination to Copper(I/II) Centers

As mentioned in the previous section, it is well known that the catalytic activity in ATRP is influenced by the solvent, likely due to the coordination of solvent molecules to the metal center [32,40,44,45]. Indeed, $[Cu^IL]^+$ complexes have vacancies in the coordination sphere of the metal center [8], and, depending on the ligand type, one or more solvent molecules may be able to coordinate the copper atom.

Aiming at understanding how DMSO and MeCN behave in the presence of copper complexes, a model system formed by single $Cu^{I/II}$ ions and one solvent molecule (S) was initially investigated. In principle, MeCN can coordinate using the lone pair on the N atom (*end-on* coordination) or the nitrile π system (*side-on* coordination), although this second type of coordination is less common and affords a weaker coordination mode. DMSO can coordinate with the metal center via S or O donor atoms (Figure 1).

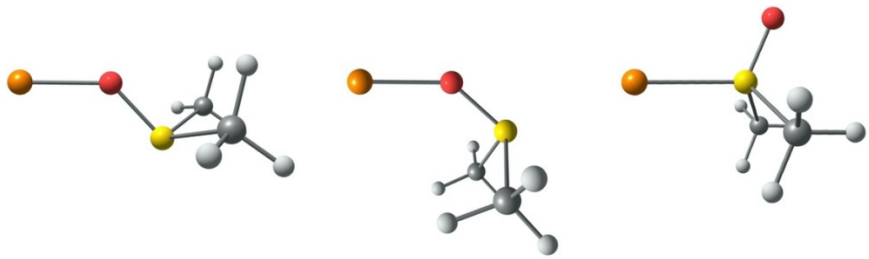

Figure 1. Fully optimized geometries of Cu^IDMSO-κOα (**left**), Cu^IDMSO-κOβ (**middle**), Cu^IDMSO-κS (**right**); level of theory: (PCM-)M06/6-311+G(d,p). Color legend: copper (orange), oxygen (red), sulfur (yellow), carbon (grey), hydrogen (light grey).

Furthermore, exploring the O-coordination modes of DMSO, two possible conformations can be found: the Cu^IDMSO-κOα, characterized by the methyl substituents pointing away from the metal and the S lone pair oriented toward the coordination sphere of the copper atom; or the Cu^IDMSO-κOβ, with the methyl substituents pointing towards the metal and the S lone pair away from it. The model systems built with Cu^I as well as with Cu^{II} ions interacting with one molecule of either MeCN or DMSO were fully optimized in

the gas phase as well as in the implicit solvent. The Gibbs free energies of the formation of these adducts are reported in Table 3.

Table 3. ΔG_r (kcal/mol) of $[Cu^{I/II}(S)]^{+/2+}$ formation from $Cu^{I/II}$ and S (S=MeCN, DMSO) calculated in gas phase and in implicit solvent; level of theory: (PCM-)M06/6-311+G(d,p).

S	Cu^{I}		Cu^{II}	
	Gas Phase	**In Solvent** [1]	**Gas Phase**	**In Solvent** [1]
MeCN (*end-on*)	−51.7	−24.8	−161.6	−38.7
DMSO-κOα	−57.5	−23.7	−208.2	−86.0
DMSO-κOβ	−56.0	−24.2	- [2]	- [2]
DMSO-κS	−35.8	−15.2	−183.6	−71.2

[1] The ΔmRTln(M/0.0409) correction with Δm = −1, already included in the reported results, is: −3.64 kcal/mol for MeCN (19 M) and −3.46 kcal/mol for DMSO (14 M). [2] In the gas phase, only α complex was obtained.

The π-coordinated acetonitrile adduct (*side-on* coordination) could not be obtained, either in the gas phase or the condensed phase, not even by constrained optimization.

According to the results reported in Table 3, the Cu^{I} center has an evident preference for coordination by DMSO-κO than by MeCN in the gas phase, while in a solvent, Cu^{I} does not discriminate much in the coordination between MeCN and DMSO-κO. The coordination of DMSO via S is disfavored in both models. On the other hand, the coordination of a solvent molecule to the Cu^{II} center is always in favor of DMSO, especially CuDMSO-κO. This is in agreement with the increased hard character of Cu^{II} with respect to Cu^{I}.

In both Cu^{I} and Cu^{II}, DMSO-κOα and DMSO-κOβ are only 1.5–0.2 kcal/mol apart, which is of the same order as *RT* at ambient conditions and close to the computational error. However, analyzing the structures of $Cu^{I/II}$ complexes having coordinated DMSO, retrieved from the Cambridge Crystallographic Database (*ca.* 340 entries) [46], CuDMSO-κOα coordination was always displayed (see, for example, [47,48]). Thus, in all the starting geometries employed in the calculations reported from now on, only this type of oxygen coordination, DMSO-κOα, was taken into consideration.

2.2.2. $Cu^{I/II}L(S)]^{+/2+}$ Complexes

Next, we expanded the simple $[Cu^{I/II}(S)]^{+/2+}$ model by introducing the effect of the ligand to describe the formation of the complexes $[Cu^{I/II}L(S)]^{+/2+}$. The main difference between the ligands here discussed is that PMDETA acts as a tridentate ligand, while both Me_6TREN and TPMA can occupy four coordination sites around the copper ions. Furthermore, one should keep in mind that the copper(I) complexes are usually $18e^{-}$, tetracoordinated species with distorted tetrahedral coordination geometry, while the copper(II) ones are often pentacoordinated with trigonal bipyramidal or tetragonal pyramidal arrangements, depending on the ligand set. The structural features of copper(I) and copper(II) complexes with the ligands investigated in this work have been extensively studied using several techniques and also deeply discussed in a review in 2005 [49].

Analogously to what we have reported in the previous section, we calculated ΔG_r for the coordination of MeCN and DMSO to complexes $[Cu^{I/II}L]^{+/2+}$ both in the gas phase and in the continuum solvent (see Table 4). In the case L = PMDETA, the coordination of a second molecule of solvent has also been explored, although, according to the literature, it has never been observed when crystals of PMDETA copper(I) complexes were isolated [49,50].

Having both the effect of ligands and explicit solvent molecules, we observe that it is possible to discriminate between the thermodynamic effects of the two solvents. Both in the gas phase and in the continuum solvent, MeCN appears as the stronger coordinative solvent in the case of Cu^{I}. On the other hand, the harder character of Cu^{II} privileges, once again, oxygen coordination instead of nitrogen, despite both solvents producing very stable complexes.

Table 4. ΔE_r and ΔG_r (kcal/mol) of reaction (1) calculated in gas phase and in solution; level of theory: (PCM-)M06/6-311+G(d,p).

Reaction	ΔE_r Gas Phase			ΔG_r Gas Phase			ΔG_r In Solution [1]		
	MeCN	DMSO-κO[2]	DMSO-κS	MeCN	DMSO-κO[2]	DMSO-κS	MeCN	DMSO-κO[2]	DMSO-κS
$[Cu^{I}(Me_6TREN)]^+ + S \rightleftarrows [Cu^{I}(Me_6TREN)(S)]^+$	−17.9	−20.8	−15.2	−7.5	−9.4	−2.6	−4.4	−2.2	0.4
$[Cu^{I}(PMDETA]^+ + S \rightleftarrows [Cu^{I}(PMDETA)(S)]^+$	−23.0	−24.2	−19.6	−12.6	−11.6	−5.5	−6.3	−3.3	−2.6
$[Cu^{I}(PMDETA)(S)]^+ + S \rightleftarrows [Cu^{I}(PMDETA)(S)_2]^+$	−11.4	−18.2	-	−1.8	−6.4	-	1.7	0.2	-
$[Cu^{I}(TPMA)]^+ + S \rightleftarrows [Cu^{I}(TPMA)(S)]^+$	−16.8	−18.9	−13.6	−6.7	−7.5	−1.8	−4.0	−2.7	−0.4
$[Cu^{II}(Me_6TREN)]^{2+} + S \rightleftarrows [Cu^{II}(Me_6TREN)(S)]^{2+}$	−44.7	−55.6	−30.5	−33.9	−41.8	−16.1	−10.1	−32.2	−11.7
$[Cu^{II}(PMDETA)]^{2+} + S \rightleftarrows [Cu^{II}(PMDETA)(S)]^{2+}$	−48.7	−60.3	-	−36.6	−46.1	-	−18.7	−31.0	-
$[Cu^{II}(PMDETA)(S)]^{2+} + S \rightleftarrows [Cu^{II}(PMDETA)(S)_2]^{2+}$	−29.1	−38.5	-	−18.5	−24.2	-	−6.3	−17.0	-
$[Cu^{II}(TPMA)]^{2+} + S \rightleftarrows [Cu^{II}(TPMA)(S)]^{2+}$	−43.7	−52.7	−32.0	−31.8	−39.5	−18.3	−19.1	−29.6	−15.7

[1] The $\Delta m RT \ln(M/0.0409)$ correction with $\Delta m = -1$, already included in the reported results, is: −3.64 kcal/mol for MeCN (19 M) and −3.46 kcal/mol for DMSO (14 M). [2] DMSO-κOα.

The nature of the ligand plays an important role in the stabilization effect of the solvent for both Cu^{I} and Cu^{II} complexes, which is always greater in the latter case.

$[Cu^{I}(PMDETA)]^+$ gives the most stable complex with a single molecule of acetonitrile. The coordination of a second molecule of MeCN, however, is disfavored in the continuum solvent but favored in the gas phase. The very same effect is observed in the case of DMSO. Similarly to what was observed for $[Cu^{I/II}(S)]^{+/2+}$ (Table 3), coordination via DMSO-κS is disfavored when compared to DMSO-κO.

A survey of the data reported in Table 4 highlights the importance of considering both the implicit and explicit solvent effects for the correct description of the thermodynamics of this class of copper complexes. This aspect is evident in the coordination of the second molecule of solvent in $[Cu^{I}(PMDETA)]^+$. Indeed, although this coordination appears as stabilizing in the gas phase, it turns out to be unstable when also the implicit polar medium is accounted for, in agreement with the crystallographic observations [50].

2.2.3. Analysis of the Isomers $[Cu^{II}(PMDETA)X(S)]^+$

The $Cu^{I/II}$ complexes with PMDETA deserve further discussion. The metal center in $[Cu^{I}PMDETA(S)]^+$ has a structure close to a distorted tetrahedron, where three positions are occupied by PMDETA and the fourth is saturated by one solvent molecule (see Chart 1). From the calculations presented in Table 4 and the crystallographic information [50], we have excluded the possibility of the formation of a pentacoordinated complex through coordination with a second solvent molecule. This aspect makes $[Cu^{I}PMDETA(S)]^+$ a special case because the reaction with an initiator can produce four different isomers (Figure 2), depending on the direction of halogenation. Despite that few crystallographic data are available for the structure of $[Cu^{II}(PMDETA)X(S)]^+$ complexes [51], we decided to further investigate this aspect.

Four $[Cu^{II}(PMDETA)Br(S)]^+$ isomers (denoted as *In* with n = 1, 2, 3, 4) were studied to this end (see Figure 2, Tables 5, S6 and S7 for geometry parameters). The complexes differ in the positions of the halide ion and solvent molecule coordinated by the metal center and the methyl group attached to the central nitrogen atom.

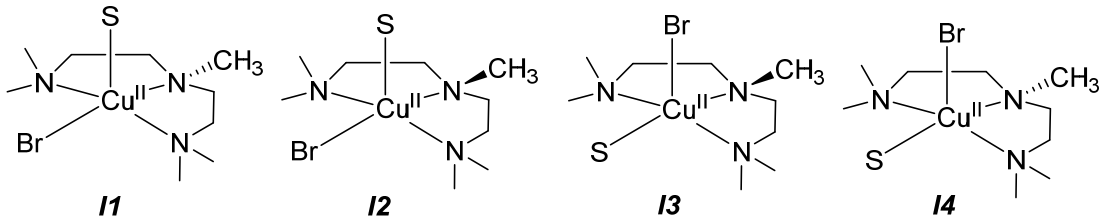

Figure 2. Possible isomers of $[Cu^{II}(PMDETA)Br(S)]^+$, with S = MeCN or DMSO.

Table 5. ΔG_r (kcal/mol) of the coordination reaction of $[Cu^{II}(PMDETA)Br]^+$ with a solvent molecule calculated in gas phase and in implicit solvent; level of theory: (PCM-)M06/6-311+G(d,p).

Isomer	$[Cu^{II}(PMDETA)Br]^+$ + MeCN ⇄ $[Cu^{II}(PMDETA)Br(MeCN)]^+$			$[Cu^{II}(PMDETA)Br]^+$ + DMSO ⇄ $[Cu^{II}(PMDETA)Br(DMSO)]^+$		
	ΔE_r Gas Phase	ΔG_r Gas Phase	ΔG_r In MeCN [1]	ΔE_r Gas Phase	ΔG_r Gas Phase	ΔG_r In DMSO [1]
I1	−15.9	−2.3	4.4	−25.6	−11.0	−0.5
I2	−19.4	−8.1	−1.1	−29.7	−15.1	−4.7
I3	−11.2	0.5	4.6	−25.7	−11.7	−3.9
I4	−6.1	5.5	10.6	−17.8	−3.3	4.5

[1] The ΔmRTln(M/0.0409) correction with Δm = −1 is: −3.64 kcal/mol for MeCN (19 M) and −3.46 kcal/mol for DMSO (14 M).

In good accordance with the crystallographic data, *I2* was calculated as the most stable isomer in both MeCN and DMSO (see Table 5) [52]. In DMSO (implicit solvation), *I2* is clearly the most stable isomer, even if the existence of other isomers should not be excluded. On the other hand, in MeCN (implicit solvation), *I2* appears as the only thermodynamically stable isomer.

2.3. Reactions including the Explicit Solvent Coordination

With the results reported in Tables 4 and 5, we have shown that the coordination of one molecule of solvent is an important aspect to consider for the stability of Cu^I and Cu^{II} complexes. Moreover, we have also proven the importance of considering both implicit and explicit solvent descriptions in computational models.

Based on these considerations, we have recalculated ΔG_r for the ATRP process, described by Equations (4) and (5), including the effect of the explicit coordination of the solvent. The free energies of the reaction are reported in Table 6. Concerning Equation (5), the sole $[Cu^I(PMDETA)(DMSO\text{-}\kappa O\alpha)]^+$ was considered in the reactants in DMSO, whereas only $[Cu^{II}(PMDETA)X(S)]^+$ (*I2*) was considered as a product in both solvents (see Tables 4 and 5).

$$RX + \left[Cu^{I}L(S)\right]^{+} \rightleftarrows \left[Cu^{II}LX\right]^{+} + S + R^{\bullet} \quad (4)$$

$$RX + \left[Cu^{I}(PMDETA)(S)\right]^{+} \rightleftarrows \left[Cu^{II}(PMDETA)X(S)\right]^{+} + R^{\bullet} \quad (5)$$

As reported in Table 6, accounting for the coordination of the solvent drastically affects the thermodynamic analysis for ATRP reactions performed in different media. The predicted activities are, in most of the cases, in good agreement with the experimental measurements/extrapolations [9]. The most striking result is that the computed value of K_{ATRP} in DMSO is 1–2 orders of magnitude higher than in MeCN, a prediction matching the experimental observations [9,32,40]. Moreover, the trend of K_{ATRP} with respect to the ligands is the same as observed experimentally, which means that the activity follows the order PMDETA < TPMA < Me_6TREN in acetonitrile and PMDETA ≈ TPMA < Me_6TREN in DMSO, if we consider reaction (4). In the case of PMDETA, we have also calculated the energetics for reaction (5), considering that a solvent molecule can remain coordinated to the

copper center after its oxidation to Cu^{II}. In this last case, the reactivity trend does not match the experimental one, especially for the DMSO data, since PMDETA appears to outperform the other catalytic systems. This is probably not so surprising considering that with PMDETA several equilibria involving both halide and solvent coordination/dissociation might be present in copper(II) species [44,49].

Table 6. ΔE_r and ΔG_r (kcal/mol) of reaction (1) calculated in gas phase and in solution; level of theory: (PCM-)M06/6-311+G(d,p).

Reaction	S = MeCN			S = DMSO		
	ΔE Gas Phase	ΔG_r Gas Phase	ΔG_r [1] In Solution	ΔE Gas Phase	ΔG_r Gas Phase	ΔG_r [1] In Solution
$[Cu^{I}(Me_6TREN)(S)]^+ + AlCl \rightleftarrows [Cu^{II}(Me_6TREN)Cl]^+ + Al^\bullet + S$	25.2	13.6	4.7	28.1	15.4	3.8
$[Cu^{I}(Me_6TREN)(S)]^+ + AlBr \rightleftarrows [Cu^{II}(Me_6TREN)Br]^+ + Al^\bullet + S$	26.1	14.5	6.2	29.0	16.4	5.4
$[Cu^{I}(Me_6TREN)(S)]^+ + EtCl^{i}Bu \rightleftarrows [Cu^{II}(Me_6TREN)Cl]^+ + Et^{i}Bu^\bullet + S$	28.6	14.9	5.1	31.5	16.7	4.2
$[Cu^{I}(Me_6TREN)(S)]^+ + EtBr^{i}Bu \rightleftarrows [Cu^{II}(Me_6TREN)Br]^+ + Et^{i}Bu^\bullet + S$	29.0	15.0	5.8	31.9	16.9	4.9
$[Cu^{I}(Me_6TREN)(S)]^+ + MeClPr \rightleftarrows [Cu^{II}(Me_6TREN)Cl]^+ + MePr^\bullet + S$	30.0	17.8	8.1	32.9	19.6	7.3
$[Cu^{I}(Me_6TREN)(S)]^+ + MeBrPr \rightleftarrows [Cu^{II}(Me_6TREN)Br]^+ + MePr^\bullet + S$	31.2	18.8	9.8	34.1	20.7	9.0
$[Cu^{I}(PMDETA)(S)]^+ + AlCl \rightleftarrows [Cu^{II}(PMDETA)Cl]^+ + Al^\bullet + S$	32.7	20.9	9.4	33.9	19.9	5.8
$[Cu^{I}(PMDETA)(S)]^+ + AlBr \rightleftarrows [Cu^{II}(PMDETA)Br]^+ + Al^\bullet + S$	33.4	21.4	10.5	34.6	20.3	7.0
$[Cu^{I}(PMDETA)(S)]^+ + EtCl^{i}Bu \rightleftarrows [Cu^{II}(PMDETA)Cl]^+ + Et^{i}Bu^\bullet + S$	36.1	22.2	9.7	37.3	21.2	6.2
$[Cu^{I}(PMDETA)(S)]^+ + EtBr^{i}Bu \rightleftarrows [Cu^{II}(PMDETA)Br]^+ + Et^{i}Bu^\bullet + S$	36.3	21.8	10.1	37.5	20.8	6.6
$[Cu^{I}(PMDETA)(S)]^+ + MeClPr \rightleftarrows [Cu^{II}(PMDETA)Cl]^+ + MePr^\bullet + S$	37.5	25.1	12.8	38.7	24.1	9.2
$[Cu^{I}(PMDETA)(S)]^+ + MeBrPr \rightleftarrows [Cu^{II}(PMDETA)Br]^+ + MePr^\bullet + S$	38.5	25.7	14.1	39.7	24.7	10.6
$[Cu^{I}(TPMA)(S)]^+ + AlCl \rightleftarrows [Cu^{II}(TPMA)Cl]^+ + Al^\bullet + S$	27.1	15.7	7.3	29.2	16.4	5.9
$[Cu^{I}(TPMA)(S)]^+ + AlBr \rightleftarrows [Cu^{II}(TPMA)Br]^+ + Al^\bullet + S$	27.6	16.3	8.5	29.7	17.0	7.1
$[Cu^{I}(TPMA)(S)]^+ + EtCl^{i}Bu \rightleftarrows [Cu^{II}(TPMA)Cl]^+ + Et^{i}Bu^\bullet + S$	30.6	17.0	7.6	32.6	17.7	6.2
$[Cu^{I}(TPMA)(S)]^+ + EtBr^{i}Bu \rightleftarrows [Cu^{II}(TPMA)Br]^+ + Et^{i}Bu^\bullet + S$	30.5	16.8	8.1	32.6	17.5	6.7
$[Cu^{I}(TPMA)(S)]^+ + MeClPr \rightleftarrows [Cu^{II}(TPMA)Cl]^+ + MePr^\bullet + S$	31.9	19.9	10.7	34.0	20.6	9.3
$[Cu^{I}(TPMA)(S)]^+ + MeBrPr \rightleftarrows [Cu^{II}(TPMA)Cl]^+ + MePr^\bullet + S$	32.7	20.6	12.1	34.8	21.3	10.7
$[Cu^{I}(PMDETA)(S)]^+ + AlCl \rightleftarrows [Cu^{II}(PMDETA)Cl(S)]^+ + Al^\bullet$	15.0	12.4	5.8	2.7	4.6	−1.0
$[Cu^{I}(PMDETA)(S)]^+ + AlBr \rightleftarrows [Cu^{II}(PMDETA)Br(S)]^+ + Al^\bullet$	14.0	14.3	9.4	4.9	5.2	2.4
$[Cu^{I}(PMDETA)(S)]^+ + EtCl^{i}Bu \rightleftarrows [Cu^{II}(PMDETA)Cl(S)]^+ + Et^{i}Bu^\bullet$	18.5	13.6	6.1	6.1	5.9	−0.7
$[Cu^{I}(PMDETA)(S)]^+ + EtBr^{i}Bu \rightleftarrows [Cu^{II}(PMDETA)Br(S)]^+ + Et^{i}Bu^\bullet$	16.9	13.8	9.0	7.8	5.7	2.0
$[Cu^{I}(PMDETA)(S)]^+ + MeClPr \rightleftarrows [Cu^{II}(PMDETA)Cl(S)]^+ + MePr^\bullet$	19.8	16.6	9.2	7.5	8.8	2.4
$[Cu^{I}(PMDETA)(S)]^+ + MeBrPr \rightleftarrows [Cu^{II}(PMDETA)Br(S)]^+ + MePr^\bullet$	19.1	17.6	13.0	10.0	9.6	6.0

[1] The ΔmRTln(M/0.0409) correction with Δm = 1, already included in the reported results, is: 3.64 kcal/mol for MeCN (19 M) and 3.46 kcal/mol for DMSO (14 M).

The calculated activity of the initiator follows the order MeXP < EtX^{i}Bu ≈ AlX for any given ligand, which fairly matches the experimental trend. The only discrepancy between the predicted and experimental data regards the effect of the halide substituent in the initiator: the reactions involving chloro-derivatives appear to be the most active (smaller ΔG_r), but this is not the trend observed experimentally. However, we must remember that in calculations performed with solvents treated as continuum dielectric constants, the mean unsigned error on solvation-free energy can be of the order of 1 kcal/mol for neutral systems, while for ionic species, the error can increase to the order of a few kcal/mol [53,54]. The systematic inverted trend between bromine and chlorine may be an indication that other solvent interactions could affect the activity of the initiators and, particularly, the stability of the transition state.

3. Materials and Methods

All the calculations were performed using Gaussian 09, Revision B.01 [55]. After testing several functionals for the ligands Me_6TREN, PMDETA and TPMA and the $[Cu^I(Me_6TREN)]^+$ and $[Cu^I(TPMA)]^+$ complexes, the level of theory M06/6-311+G(d,p) was selected as most suitable for the present study [56]. The structural benchmarking was based on the comparison of selected interatomic distances and angles to those measured in analogous compounds taken from the Cambridge Structural Database. Relevant structural parameters are included in the Supporting Information. All geometry optimizations were carried out without any constraints, and frequency calculations, performed at the same level of theory, were conducted to assess the nature of the stationary points (all positive frequencies). Thermodynamic data (ΔG_r) at 298.15 K and 1 atm were calculated from electronic energies and frequency computations using standard statistical mechanics relationships for an ideal gas. Solvent effects were accounted for using the polarizable continuum model (PCM). A standard cavity was used, and the values of the dielectric constants used for acetonitrile (MeCN) and dimethyl sulfoxide (DMSO) were 37.5 and 46.7, respectively. To account for the correct thermodynamic effect given by the solvent, energies relative to the passage from 1 mol/L in the gas phase to 1 mol/L in solution, given by the term $\Delta m RT \ln(M/0.0409)$, were added as a correction to all free energies calculated in PCM. Δm is the change in number of moles of solvated species in the reaction, and R and T are the universal gas constant [L·bar/K·mol] and the temperature [K], respectively. M is the molarity of the solvent in the liquid phase, which is 19 M for MeCN and 14 M for DMSO. The value 0.0409 stands for the quotient P/RT, where P is the pressure at 1 atm. For $\Delta m = 1$, the corrective terms are 3.64 kcal/mol for MeCN (19 M) and 3.46 kcal/mol for DMSO (14 M) [53,54,57]. Orbital analysis was carried out using the GaussSum software package [58].

4. Conclusions

The effects of solvent coordination on the ATRP equilibrium constants were investigated through computational methods. Both acetonitrile (MeCN) and dimethyl sulfoxide (DMSO) were found to be coordinating solvents, but with very different strengths. The greater affinity of Cu(I) to nitrogen atoms and the larger size of DMSO are decisive factors. The different coordinative attitudes of the two solvents towards $[Cu^I(L)]^+$ complexes affect the final ATRP ΔG_r, modifying the equilibrium constant K_{ATRP}.

Only when both the implicit (PCM) and explicit (solvent molecule(s)) effects of the solvent were considered, was it possible to establish a more reliable solvation effect on the thermodynamics of the ATRP reaction performed in different media. In particular, it enabled us to explain why K_{ATRP} is 1–2 orders of magnitude greater in DMSO than in MeCN.

Supplementary Materials: The following supporting information can be downloaded at: https://www.mdpi.com/article/10.3390/catal12121656/s1: Table S1: Cu-ligand relative contribution in the HOMO-LUMO orbitals of $[Cu^{I}(Me_6TREN)]^+$, $[Cu^{I}(PMDETA)]^+$ and $[Cu^{I}(TPMA)]^+$, calculated at different levels of theory; Table S2: Interatomic distances [Å] and angles [°] in the Cu^{I} and Cu^{II} complexes with the Me_6TREN ligand (L); level of theory: M06/6-311+G(d,p); Table S3: Interatomic distances [Å] and angles [°] in the Cu^{I} and Cu^{II} complexes with the PMDETA ligand (L); level of theory: M06/6-311+G(d,p); Table S4: Interatomic distances [Å] and angles [°] in the Cu^{I} and Cu^{II} complexes with the TPMA ligand (L); level of theory: M06/6-311+G(d,p); Table S5: ΔE_r and ΔG_r [kcal/mol] for the R-X (X=Cl or Br) homolytic cleavage in gas phase and in solvent; level of theory (PCM-)M06/6-311+G(d,p); Figure S1: Energy profile of the Cu^{I}-N-C angle in gas phase (green) and in acetonitrile (blu); level of theory: (PCM-)M06/6-311+G(d,p); Table S6: Cu-Br and Cu-solvent interatomic distances [Å] in the $[Cu^{II}(PMDETA)Br(MeCN)]^+$ complexes calculated in gas phase and in solvent (in parenthesis); level of theory: (PCM-)M06/6-311+G(d,p); Table S7: Cu-Br and Cu-solvent interatomic distances [Å] in the $[Cu^{II}(PMDETA)Br(DMSO\text{-}\kappa O\alpha)]^+$ complexes calculated in gas phase and in solvent (in parenthesis); level of theory: (PCM-)M06/6-311+G(d,p); Cartesian coordinates.

Author Contributions: Conceptualization, A.A.I., L.O. and A.G.; methodology, L.O.; validation, S.R. and L.O.; formal analysis, S.R.; investigation, S.R.; resources, L.O.; data curation, S.R., L.O. and C.T.; writing—original draft preparation, S.R. and A.A.I.; writing—review and editing, S.R., L.O., A.A.I. and C.T.; visualization, S.R.; supervision, A.A.I. and L.O.; funding acquisition, A.A.I. and L.O. All authors have read and agreed to the published version of the manuscript.

Funding: This research was funded by Università degli Studi di Padova and CINECA (ISCRA grant number HP10C6S18Z, project acronym STREGA, "Filling the STructure-REactivity GAp: in silico multiscale approaches to rationalize the design of molecular catalysts"), PI: L.O.

Data Availability Statement: The data presented in this study are available in the article and Supporting Materials.

Conflicts of Interest: The authors declare no conflict of interest.

References

1. Matyjaszewski, K.; Xia, J. Atom Transfer Radical Polymerization. *Chem. Rev.* **2001**, *101*, 2921–2990. [CrossRef] [PubMed]
2. Matyjaszewski, K. Atom Transfer Radical Polymerization (ATRP): Current Status and Future Perspectives. *Macromolecules* **2012**, *45*, 4015–4039. [CrossRef]
3. Matyjaszewski, K. Advanced Materials by Atom Transfer Radical Polymerization. *Adv. Mater.* **2018**, *30*, 1706441. [CrossRef] [PubMed]
4. Ribelli, T.G.; Lorandi, F.; Fantin, M.; Matyjaszewski, K. Atom Transfer Radical Polymerization: Billion Times More Active Catalysts and New Initiation Systems. *Macromol. Rapid Commun.* **2019**, *40*, 1800616. [CrossRef] [PubMed]
5. Lin, C.Y.; Coote, M.L.; Gennaro, A. Ab Initio Evaluation of the Thermodynamic and Electrochemical Properties of Alkyl Halides and Radicals and Polymerization. *J. Am. Chem. Soc.* **2008**, *130*, 12762–12774. [CrossRef] [PubMed]
6. De Paoli, P.; Isse, A.A.; Bortolamei, N.; Gennaro, A. New Insights into the Mechanism of Activation of Atom Transfer Radical Polymerization by Cu(I) Complexes. *Chem. Commun.* **2011**, *47*, 3580–3582. [CrossRef] [PubMed]
7. Isse, A.A.; Bortolamei, N.; De Paoli, P.; Gennaro, A. On the Mechanism of Activation of Copper-Catalyzed Atom Transfer Radical Polymerization. *Electrochim. Acta* **2013**, *110*, 655–662. [CrossRef]
8. Tang, W.; Tsarevsky, N.V.; Matyjaszewski, K. Determination of Equilibrium Constants for Atom Transfer Radical Polymerization. *J. Am. Chem. Soc.* **2006**, *128*, 1598–1604. [CrossRef]
9. Tang, W.; Kwak, Y.; Braunecker, W.; Tsarevsky, N.V.; Coote, M.L.; Matyjaszewski, K. Understanding Atom Transfer Radical Polymerization: Effect of Ligand and Initiator Structures on the Equilibrium Constants. *J. Am. Chem. Soc.* **2008**, *130*, 10702–10713. [CrossRef]
10. Pan, X.; Fantin, M.; Yuan, F.; Matyjaszewski, K. Externally Controlled Atom Transfer Radical Polymerization. *Chem. Soc. Rev.* **2018**, *47*, 5457–5490. [CrossRef]
11. Min, K.; Gao, H.; Matyjaszewski, K. Use of Ascorbic Acid as Reducing Agent for Synthesis of Well-Defined Polymers by ARGET ATRP. *Macromolecules* **2007**, *40*, 1789–1791. [CrossRef]
12. Simakova, A.; Averick, S.E.; Konkolewicz, D.; Matyjaszewski, K. Aqueous ARGET ATRP. *Macromolecules* **2012**, *45*, 6371–6379. [CrossRef]
13. Mendonça, P.V.; Ribeiro, J.P.M.; Abreu, C.M.R.; Guliashvili, T.; Serra, A.C.; Coelho, J.F.J. Thiourea Dioxide as a Green and Affordable Reducing Agent for the ARGET ATRP of Acrylates, Methacrylates, Styrene, Acrylonitrile, and Vinyl Chloride. *ACS Macro Lett.* **2019**, *8*, 315–319. [CrossRef] [PubMed]

14. Abreu, C.M.R.; Serra, A.C.; Popov, A.V.; Matyjaszewski, K.; Guliashvili, T.; Coelho, J.F.J. Ambient Temperature Rapid SARA ATRP of Acrylates and Methacrylates in Alcohol–Water Solutions Mediated by a Mixed Sulfite/Cu(II)Br_2 Catalytic System. *Polym. Chem.* **2013**, *4*, 5629–5636. [CrossRef]
15. Mendes, J.P.; Branco, F.; Abreu, C.M.R.; Mendonça, P.V.; Serra, A.C.; Popov, A.V.; Guliashvili, T.; Coelho, J.F.J. Sulfolane: An Efficient and Universal Solvent for Copper-Mediated Atom Transfer Radical (Co)Polymerization of Acrylates, Methacrylates, Styrene, and Vinyl Chloride. *ACS Macro Lett.* **2014**, *3*, 858–861. [CrossRef]
16. Lorandi, F.; Fantin, M.; Isse, A.A.; Gennaro, A. RDRP in the Presence of Cu0: The Fate of Cu(I) Proves the Inconsistency of SET-LRP Mechanism. *Polymer* **2015**, *72*, 238–245. [CrossRef]
17. Matyjaszewski, K.; Jakubowski, W.; Min, K.; Tang, W.; Huang, J.; Braunecker, W.A.; Tsarevsky, N.V. Diminishing Catalyst Concentration in Atom Transfer Radical Polymerization with Reducing Agents. *Proc. Natl. Acad. Sci. USA* **2006**, *103*, 15309–15314. [CrossRef]
18. Konkolewicz, D.; Magenau, A.J.D.; Averick, S.E.; Simakova, A.; He, H.; Matyjaszewski, K. ICAR ATRP with Ppm Cu Catalyst in Water. *Macromolecules* **2012**, *45*, 4461–4468. [CrossRef]
19. Tasdelen, M.A.; Uygun, M.; Yagci, Y. Photoinduced Controlled Radical Polymerization. *Macromol. Rapid Commun.* **2011**, *32*, 58–62. [CrossRef]
20. Konkolewicz, D.; Schröder, K.; Buback, J.; Bernhard, S.; Matyjaszewski, K. Visible Light and Sunlight Photoinduced ATRP with Ppm of Cu Catalyst. *ACS Macro Lett.* **2012**, *1*, 1219–1223. [CrossRef]
21. Anastasaki, A.; Nikolaou, V.; Zhang, Q.; Burns, J.; Samanta, S.R.; Waldron, C.; Haddleton, A.J.; McHale, R.; Fox, D.; Percec, V.; et al. Copper(II)/Tertiary Amine Synergy in Photoinduced Living Radical Polymerization: Accelerated Synthesis of ω-Functional and α,ω-Heterofunctional Poly(Acrylates). *J. Am. Chem. Soc.* **2014**, *136*, 1141–1149. [CrossRef] [PubMed]
22. Magenau, A.J.D.; Strandwitz, N.C.; Gennaro, A.; Matyjaszewski, K. Electrochemically Mediated Atom Transfer Radical Polymerization. *Science* **2011**, *332*, 81–84. [CrossRef] [PubMed]
23. Fantin, M.; Isse, A.A.; Gennaro, A.; Matyjaszewski, K. Understanding the Fundamentals of Aqueous ATRP and Defining Conditions for Better Control. *Macromolecules* **2015**, *48*, 6862–6875. [CrossRef]
24. Lorandi, F.; Fantin, M.; Isse, A.A.; Gennaro, A. Electrochemically Mediated Atom Transfer Radical Polymerization of N-Butyl Acrylate on Non-Platinum Cathodes. *Polym. Chem.* **2016**, *7*, 5357–5365. [CrossRef]
25. Chmielarz, P.; Fantin, M.; Park, S.; Isse, A.A.; Gennaro, A.; Magenau, A.J.D.; Sobkowiak, A.; Matyjaszewski, K. Electrochemically Mediated Atom Transfer Radical Polymerization (eATRP). *Prog. Polym. Sci.* **2017**, *69*, 47–78. [CrossRef]
26. Isse, A.A.; Gennaro, A. Electrochemistry for Atom Transfer Radical Polymerization. *Chem. Rec.* **2021**, *21*, 2203–2222. [CrossRef]
27. Zaborniak, I.; Chmielarz, P. Ultrasound-Mediated Atom Transfer Radical Polymerization (ATRP). *Materials* **2019**, *12*, 3600. [CrossRef]
28. Kaur, A.; Ribelli, T.G.; Schröder, K.; Matyjaszewski, K.; Pintauer, T. Properties and ATRP Activity of Copper Complexes with Substituted Tris(2-Pyridylmethyl)Amine-Based Ligands. *Inorg. Chem.* **2015**, *54*, 1474–1486. [CrossRef]
29. Melville, J.N.; Bernhardt, P.V. Electrochemical Exploration of Active Cu-Based Atom Transfer Radical Polymerization Catalysis through Ligand Modification. *Inorg. Chem.* **2021**, *60*, 9709–9719. [CrossRef]
30. Wang, Y.; Kwak, Y.; Buback, J.; Buback, M.; Matyjaszewski, K. Determination of ATRP Equilibrium Constants under Polymerization Conditions. *ACS Macro Lett.* **2012**, *1*, 1367–1370. [CrossRef]
31. Morick, J.; Buback, M.; Matyjaszewski, K. Effect of Pressure on Activation–Deactivation Equilibrium Constants for ATRP of Methyl Methacrylate. *Macromol. Chem. Phys.* **2012**, *213*, 2287–2292. [CrossRef]
32. Horn, M.; Matyjaszewski, K. Solvent Effects on the Activation Rate Constant in Atom Transfer Radical Polymerization. *Macromolecules* **2013**, *46*, 3350–3357. [CrossRef]
33. Smolne, S.; Buback, M. Kinetic Investigations of Cu-Mediated ATRP in Aqueous Solution. *Macromol. Chem. Phys.* **2015**, *216*, 894–902. [CrossRef]
34. Pavan, P.; Lorandi, F.; De Bon, F.; Gennaro, A.; Isse, A.A. Enhancement of the Rate of Atom Transfer Radical Polymerization in Organic Solvents by Addition of Water: An Electrochemical Study. *ChemElectroChem* **2021**, *8*, 2450–2458. [CrossRef]
35. Coullerez, G.; Malmström, E.; Jonsson, M. Solvent Effects on the Redox Properties of Cu Complexes Used as Mediators in Atom Transfer Radical Polymerization. *J. Phys. Chem. A* **2006**, *110*, 10355–10360. [CrossRef]
36. Gillies, M.B.; Matyjaszewski, K.; Norrby, P.-O.; Pintauer, T.; Poli, R.; Richard, P. A DFT Study of R−X Bond Dissociation Enthalpies of Relevance to the Initiation Process of Atom Transfer Radical Polymerization. *Macromolecules* **2003**, *36*, 8551–8559. [CrossRef]
37. Braunecker, W.A.; Brown, W.C.; Morelli, B.C.; Tang, W.; Poli, R.; Matyjaszewski, K. Origin of Activity in Cu-, Ru-, and Os-Mediated Radical Polymerization. *Macromolecules* **2007**, *40*, 8576–8585. [CrossRef]
38. Isse, A.A.; Gennaro, A.; Lin, C.Y.; Hodgson, J.L.; Coote, M.L.; Guliashvili, T. Mechanism of Carbon−Halogen Bond Reductive Cleavage in Activated Alkyl Halide Initiators Relevant to Living Radical Polymerization: Theoretical and Experimental Study. *J. Am. Chem. Soc.* **2011**, *133*, 6254–6264. [CrossRef]
39. Ribelli, T.G.; Wahidur Rahaman, S.M.; Daran, J.C.; Krys, P.; Matyjaszewski, K.; Poli, R. Effect of Ligand Structure on the Cu^{II}–R OMRP Dormant Species and Its Consequences for Catalytic Radical Termination in ATRP. *Macromolecules* **2016**, *49*, 7749–7757. [CrossRef]
40. Braunecker, W.A.; Tsarevsky, N.V.; Gennaro, A.; Matyjaszewski, K. Thermodynamic Components of the Atom Transfer Radical Polymerization Equilibrium: Quantifying Solvent Effects. *Macromolecules* **2009**, *42*, 6348–6360. [CrossRef]

41. Lanzalaco, S.; Fantin, M.; Scialdone, O.; Galia, A.; Isse, A.A.; Gennaro, A.; Matyjaszewski, K. Atom Transfer Radical Polymerization with Different Halides (F, Cl, Br, and I): Is the Process "Living" in the Presence of Fluorinated Initiators? *Macromolecules* **2017**, *50*, 192–202. [CrossRef]
42. Hildenbrand, D.L.; Lau, K.H. Dissociation Energies of the Cu and Ag Monohalides and of Ni Monofluoride. *J. Phys. Chem. A* **2006**, *110*, 11886–11889. [CrossRef] [PubMed]
43. Isse, A.A.; Lin, C.Y.; Coote, M.L.; Gennaro, A. Estimation of Standard Reduction Potentials of Halogen Atoms and Alkyl Halides. *J. Phys. Chem. B* **2011**, *115*, 678–684. [CrossRef] [PubMed]
44. Zerk, T.J.; Bernhardt, P.V. Solvent Dependent Anion Dissociation Limits Copper(I) Catalysed Atom Transfer Reactions. *Dalton Trans.* **2013**, *42*, 11683–11694. [CrossRef]
45. Zerk, T.J.; Martinez, M.; Bernhardt, P.V. A Kinetico-Mechanistic Study on Cu^{II} Deactivators Employed in Atom Transfer Radical Polymerization. *Inorg. Chem.* **2016**, *55*, 9848–9857. [CrossRef]
46. Groom, C.R.; Bruno, I.J.; Lightfoot, M.P.; Ward, S.C. The Cambridge Structural Database. *Acta Crystallogr. Sect. B Struct. Sci. Cryst. Eng. Mater.* **2016**, *72*, 171–179. [CrossRef]
47. Odarich, I.A.; Pavlishchuk, A.V.; Kalibabchuk, V.A.; Haukka, M. Crystal Structure of μ-Oxalodi hydroxamato-Bis [(2,2′-Bipyrid yl)(Di methyl Sulfoxide-KO)Copper(II)] Bis (Perchlorate). *Acta Crystallogr. Sect. Crystallogr. Commun.* **2016**, *72*, 147–150. [CrossRef]
48. Giziroglu, E.; Aygün, M.; Sarikurkcu, C.; Kazar, D.; Orhan, N.; Firinci, E.; Soyleyici, H.C.; Gokcen, C. Synthesis, Characterization and Antioxidant Activity of New Dibasic Tridentate Ligands: X-ray Crystal Structures of DMSO Adducts of 1,3-Dimethyl-5-Acetyl-Barbituric Acid o-Hydroxybenzoyl Hydrazone Copper(II) Complex. *Inorg. Chem. Commun.* **2013**, *36*, 199–205. [CrossRef]
49. Pintauer, T.; Matyjaszewski, K. Structural Aspects of Copper Catalyzed Atom Transfer Radical Polymerization. *Coord. Chem. Rev.* **2005**, *249*, 1155–1184. [CrossRef]
50. Scott, M.J.; Holm, R.H. Molecular Assemblies Containing Linear and Bent [FeIII-CN-CuII] Bridge Units: Synthesis, Structures, and Relevance to Cyanide-Inhibited Heme-Copper Oxidases. *J. Am. Chem. Soc.* **1994**, *116*, 11357–11367. [CrossRef]
51. Olguín, J.; Bernès, S.; Gasque, L. Fluoride Ion as Ligand and Hydrogen Bond Acceptor: Crystal Structures of Two Dinuclear Cuii Complexes Built on a Diazecine Template. *Crystals* **2012**, *2*, 1357–1365. [CrossRef]
52. Margraf, G.; Bats, J.W.; Wagner, M.; Lerner, H.-W. Copper(II) PMDTA and Copper(II) TMEDA Complexes: Precursors for the Synthesis of Dinuclear Dicationic Copper(II) Complexes. *Inorg. Chim. Acta* **2005**, *358*, 1193–1203. [CrossRef]
53. Marenich, A.V.; Olson, R.M.; Kelly, C.P.; Cramer, C.J.; Truhlar, D.G. Self-Consistent Reaction Field Model for Aqueous and Nonaqueous Solutions Based on Accurate Polarized Partial Charges. *J. Chem. Theory Comput.* **2007**, *3*, 2011–2033. [CrossRef] [PubMed]
54. Harvey, J.N.; Himo, F.; Maseras, F.; Perrin, L. Scope and Challenge of Computational Methods for Studying Mechanism and Reactivity in Homogeneous Catalysis. *ACS Catal.* **2019**, *9*, 6803–6813. [CrossRef]
55. Gaussian 09 Citation | Gaussian.Com. Available online: https://gaussian.com/g09citation/ (accessed on 25 May 2022).
56. Zhao, Y.; Truhlar, D.G. The M06 Suite of Density Functionals for Main Group Thermochemistry, Thermochemical Kinetics, Noncovalent Interactions, Excited States, and Transition Elements: Two New Functionals and Systematic Testing of Four M06-Class Functionals and 12 Other Functionals. *Theor. Chem. Acc.* **2008**, *120*, 215–241. [CrossRef]
57. Skyner, R.E.; McDonagh, J.L.; Groom, C.R.; van Mourik, T.; Mitchell, J.B.O. A Review of Methods for the Calculation of Solution Free Energies and the Modelling of Systems in Solution. *Phys. Chem. Chem. Phys.* **2015**, *17*, 6174–6191. [CrossRef]
58. O'boyle, N.M.; Tenderholt, A.L.; Langner, K.M. Cclib: A Library for Package-Independent Computational Chemistry Algorithms. *J. Comput. Chem.* **2008**, *29*, 839–845. [CrossRef]